SPACE WEATHERING EFFECTS ON MERCURIAN SURFACE ANALOGS: INSIGHTS FROM COORDINATED SPECTRAL, MICROSTRUCTURAL, AND CHEMICAL ANALYSES. A. Shackelford[1], K. L. Donaldson Hanna[1], J. Gillis-Davis[2], Z. Rahman[3], B. A. Cymes[3], R. Christoffersen[3], L. P. Keller[4]. [1]University of Central Florida, 4111 Libra Drive, Orlando, FL 32816, [2]Washington University, One Brookings Drive, St. Louis, MO 63130, [3]Amentum, NASA Johnson Space Center, Houston TX, 77058, [4]NASA Johnson Space Center, Houston TX, 70058. (autumn.shackelford@ucf.edu).

Introduction: Nanophase iron (npFe) is known to be the cause of increasing optical maturity (spectral reddening, an overall darkening, and decreasing prominence of spectral features) on the Moon and S-type asteroids [e.g., 1, 2], but what happens when Fe is in short supply? How do highly reduced surfaces behave in a harsh space weathering environment? MESSENGER observations of Mercury found no features due to Fe^{2+} in visible-to-near-infrared (VNIR) spectra of the surface [e.g., 3], and other instruments confirmed that the surface contained less than 1% FeO [e.g., 4, 5]. If npFe is an unlikely space weathering product on reduced bodies [6], could carbon play a role in the optical and microstructural maturation of these regoliths?

Carbon is hypothesized to be present as a darkening agent on the surface of Mercury and on carbonaceous asteroids [e.g., 7, 8]. On Mercury, this carbon may be exogenic material introduced by impactors [9] or endogenic material excavated from a theorized graphite floatation crust [7]. Carbon may exist in concentrations of up to 5 wt. % both within Mercury's low reflectance material and throughout carbonaceous asteroids [10, 11]. To better understand the role carbon may play in space weathering on Mercury and C-type asteroids, we utilized pulsed laser irradiation to simulate aspects of micrometeorite bombardment on powders of low- to no-iron silicates mixed with C-bearing opaques.

We present VNIR reflectance spectra from 0.3-2.5 µm, transmission electron microscopy (TEM), and energy dispersive X-ray spectroscopy (EDS) analyses of two select samples from our sample suite.

Samples and Methods: *Sample Suite.* This abstract focuses on two analogs from our sample suite of twelve: (1) San Carlos olivine (SCO, < 75 µm), to use as a testbed/proof of concept for its frequent use in space weathering experiments and (2) a mixture of 95 wt. % synthetic enstatite (ENST+CB, < 80 µm) and 5 wt. % of carbon black (< 1 µm). The enstatite was produced by MatExcel and contains 0.03 wt. % Fe.

Simulated Space Weathering. Two lasers of differing pulse widths (6 ns and 100 ns) were used to simulate aspects of micrometeorite bombardment on our samples using the Washington University Laser Space Weathering Laboratory [12]. Each sample was weathered at ~10^{-7} torr for the amount of time it takes for San Carlos olivine to reach VNIR optical maturity [7] with this experimental setup.

Results: *VNIR Spectral Results.* VNIR spectra from 0.3-2.5 µm are presented in **Figure 1** for our SCO and ENST+CB samples. The pure enstatite sample (ENST) is shown for comparison and to illustrate the lack of 1-µm feature due to Fe^{2+}. As expected, the SCO spectrum darkens (~76% decrease @ 1.05 µm), reddens (~2100% increase over 1.75-2.5 µm), and experiences reduction in prominence of the 1-µm feature. The ENST+CB spectrum darkens (~44% decrease at 0.56 µm) and reddens (~198% increase over 0.4-0.55 µm) as well, though this reddening is more complex. The ENST+CB slope in this region flipped from negative (blue) to positive (red), thereby experiencing a major change in spectral behavior.

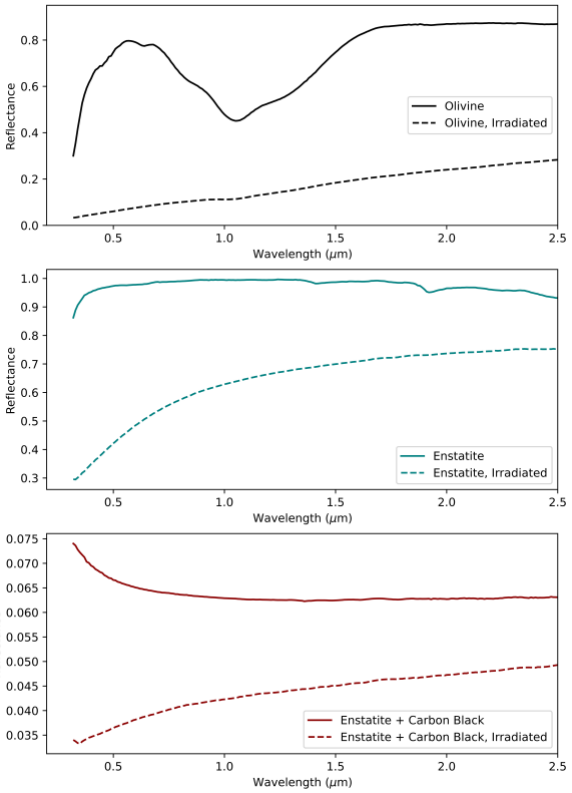

Figure 1. SCO (top), ENST (middle), and ENST+CB (bottom) spectra before and after irradiation. Note the different scales for reflectance on the y-axis for each plot. Spectra were taken by Dr. Takahiro Hiroi at RELAB.

TEM and EDS results. Both TEM and EDS data of the SCO sample show all expected, classical space weathering products. This includes a melt layer ranging from ~0.06-1.78 µm in thickness, metallic npFe of varying sizes (~8-230 nm), and concentrations, vesicles, and regions of olivine recrystallization. EDS and selected area electron diffraction (SAED) patterns show that the npFe present is likely metallic in nature, but that some of the npFe could also include Ni (**Figure 2**).

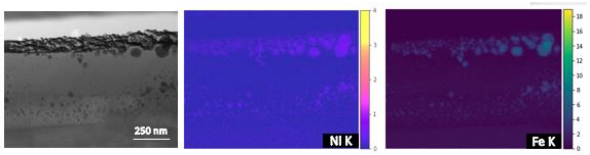

Figure 2. TEM image of SCO alongside elemental maps of Ni and Fe over the same region. The spatial correlation of Fe and Ni detections are indicative of possible npFe-Ni alloys.

Analyses of the ENST+CB sample revealed a thin melt layer (~0.03-0.24 µm) with vesicles of varying shapes and sizes dispersed in the thickest portions of the melt. No nanophase opaques are seen. We note that the melt is depleted in Si and enriched in Mg when compared to the bulk. Finally, both carbon black aggregates are noted to have trapped silicate melt splashes as a direct result of the weathering process (Figure 3).

Acknowledgments: FIB preparation and TEM/EDS analysis were performed with and supported by the NASA Facility for Astromaterials Research at Johnson Space Center under NFAR_2024_0028. This work was also directly supported by NASA's Solar System Exploration Research Virtual Institute cooperative agreement notice 80NSSC19M0214 for the Center for Lunar and Asteroid Surface Science (CLASS).

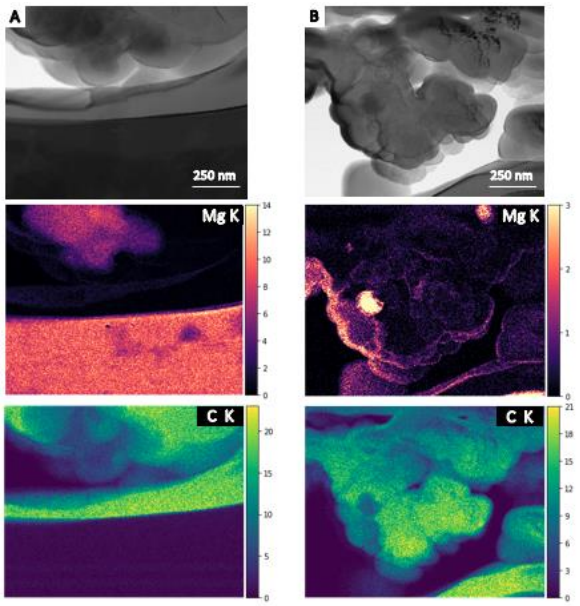

Figure 3. BF STEM images of both carbon black aggregates present above the enstatite bulk with elemental maps for Mg and C obtained via EDS. Each color bar displays normalized counts for each map to obtain better image contrast. A) Aggregate displaying Mg enrichment. B) Aggregate with distinct melt spherule embedded within, evidenced by the bright Mg-rich deposit and corresponding C-depleted region.

References: [1] Pieters & Noble (2016) *JGRP, 121,* 1865-1884. [2] Cudnik (2023) *Springer,* 943-949. [3] Warell et al. (2006) *Icarus, 180,* 281-291. [4] Evans et al. (2012), *JGRP,* 117(E12). [5] Weider et al. (2014), *Icarus,* 235, 170-186. [6] Noble & Pieters (2001). [7] Vander Kaaden & McCubbin (2015) *JGRP, 120,* 195-209. [8] Vilas and Hendrix (2020) *AGU 2020.* [9] Bruck Syal et al. (2015) *Nat. Geo., 8,* 352-356. [10] Klima et al. (2018), *GRL, 45,* 2945-2953. [11] Glavin et al. (2018), *Prim. Met. and Ast.,* 205-271. [12] Gillis-Davis (2022) *EPSC 2022, #1193.*